

Full particle orbit tracing with the RIO code in the presence of broad-spectrum MHD activity in a reversed-field pinch

This content has been downloaded from IOPscience. Please scroll down to see the full text.

2014 Nucl. Fusion 54 104007

(<http://iopscience.iop.org/0029-5515/54/10/104007>)

View [the table of contents for this issue](#), or go to the [journal homepage](#) for more

Download details:

IP Address: 128.104.165.51

This content was downloaded on 18/12/2014 at 22:28

Please note that [terms and conditions apply](#).

Full particle orbit tracing with the RIO code in the presence of broad-spectrum MHD activity in a reversed-field pinch

J.A. Reusch¹, J.K. Anderson¹ and Y. Tsidulko²

¹ Department of Physics, University of Wisconsin–Madison, 1150 University Avenue, Madison, WI 53706, USA

² Budker Institute of Nuclear Physics SB RAS and Novosibirsk State University, 630090, Novosibirsk, Russia

E-mail: jareusch@wisc.edu

Received 15 November 2013, revised 29 March 2014

Accepted for publication 2 April 2014

Published 1 October 2014

Abstract

In order to better understand the behaviour of both neutral beam injected and spontaneously generated fast ions in the Madison Symmetric Torus reversed-field pinch, we have developed the full orbit-following code random ion orbits (RIO). The low magnetic field and relatively large level of MHD activity present in MST require a full orbit code as the guiding centre assumptions are violated even for ions with modest energy. Furthermore, quasi-periodic bursts of MHD activity (sawteeth) generate large transient electric fields and significant modifications to the equilibrium magnetic fields. Understanding the full effect of these sawteeth on the spatial and velocity distribution of the fast ions is of great interest. To this end, RIO now has the ability to take the full 3D, time evolving, magnetic and electric fields produced by the visco-resistive MHD code DEBS as input. In static cases, where broad-spectrum magnetic perturbations from DEBS are input, but fixed in time, beam injected ions are found to be generally well confined with the core fast ion density profile largely unaffected by the magnetic modes while the fast ion density in the mid-radius is substantially reduced. In the dynamic case, the large amplitude magnetic fluctuations that occur at the sawtooth crash produce substantial fast ion loss. Those fast ions that are not lost are accelerated by a large, transient, parallel electric field in the co-current direction. This causes the average energy of the beam ions to increase by $\sim 20\%$, consistent with recent experimental measurements.

Keywords: reversed field pinch, energetic particles, neutral beam injection, tearing modes, particle tracing

(Some figures may appear in colour only in the online journal)

1. Introduction

Understanding fast ion dynamics is critical for designing any plasma based nuclear fusion device. While single particle motion is relatively simple to compute and understand, tracking a large number of particles and their interactions with the background plasma remains a challenge for both theory and computation. In many toroidal confinement devices this problem can be simplified somewhat by averaging over the particles gyro orbit and simply tracking the motion of the guiding centre [1, 2]. This analysis has been done using a formalism developed in [2] for the reversed-field pinch (RFP) magnetic equilibrium and all eight of the fast ion orbits identified in the tokamak equilibrium are also found in the RFP, although with somewhat modified trapped, passing and loss boundaries [3]. While the guiding centre analysis gives insight into the particle trajectories, in low field devices such as the spherical tokamak (ST) and the RFP, the gyro-orbit can

become large enough to violate the assumptions of the guiding centre formalism and the full orbit of the fast ions must be computed [4].

In the Madison Symmetric Torus (MST) RFP [5], the particle motion is further complicated by the existence of many substantial magnetic and electric field fluctuations as well as quasi-periodic magnetohydrodynamic (MHD) dynamo events known as sawteeth [6] in which large transient parallel electric fields are generated [7]. MST is a medium sized toroidal magnetic confinement device with a major radius of 150 cm and a minor radius of 52 cm. It is characterized by its circular cross section and its thick, close fitting, conducting shell. The plasma is limited by 1 cm thick toroidal graphite limiter located at the outboard mid-plane. The vacuum vessel, primary plasma facing component, structural support and single turn toroidal field coil are all provided by the 5 cm thick aluminum shell. This close fitting conducting shell has a wall time of approximately 800 ms [8], making it very nearly

an ideal conducting boundary on the time scale of a typical MST discharge (~ 80 ms with a 20 ms current flattop). This thick shell slows the onset of resistive wall modes and lends stability to the tearing modes (particularly the edge resonant $m = 0$ modes) that are present in RFP discharges in MST. Furthermore, it imposes a strong boundary condition on the poloidal flux causing the flux surfaces to tend toward Shafranov shifted nested circles. Figure 1(a) shows an example of the contours of constant poloidal flux for a 400 kA RFP discharge in MST as calculated by the equilibrium reconstruction code MSTFit [9]. A plot of the toroidal, poloidal and the magnitude of the magnetic field as a function of major radius for this equilibrium are shown in figure 1(b). Again, note that this magnetic field geometry can sustain all of the ion orbit types typically seen in tokamaks. While the low magnetic field amplitude and high shear can make the detailed 3D orbit trajectories appear somewhat strange, the poloidal projections of the orbits are very reminiscent of their tokamak counterparts, as can be seen with the example passing (red) and trapped (blue) trajectories shown in figure 1(a).

Despite this close fitting shell, when the plasma is strongly driven in the startup and sustainment phases of the discharge, strong current peaking drives the core resonant tearing mode unstable. This mode can then couple with the $m = 0, n = 1$ mode to drive an energy cascade that causes a significant increase in the fluctuation amplitudes of the rest of the tearing modes resonant in the plasma [10]. This interaction is known as the RFP sawtooth and results in strong current transport from the core to the edge of the plasma and significant toroidal flux generation [11]. This relaxation process drives the plasma toward a minimum energy state in which the parallel current is flat and the toroidal magnetic field reverses sign at the edge [12]. Figure 2(a) shows the time evolution of the RMS \tilde{B}_ϕ fluctuation amplitude for a typical 400 kA standard MST discharge. Figure 2(b) shows the \tilde{B}_ϕ spectrum of tearing mode amplitudes normalized to the average magnetic field at the wall for two time slices: between sawteeth (solid red line) and at a sawtooth crash (dashed blue line). Tearing modes are resonant inside the plasma where $\vec{k} \cdot \vec{B} = 0$ and magnetic island can form at these resonant locations. $\vec{k} \cdot \vec{B}$ can be rewritten as the safety factor $q = rB_\phi/RB_\theta = m/n$ with the resonance condition satisfied at rational values of m/n where m is the poloidal and n is the toroidal mode number. The low n mode amplitudes ($n < 5$) are dominantly from edge resonant $m = 0$ activity while the higher n modes ($n \geq 5$) are mostly $m = 1$ activity with resonant locations in the mid-radius and core regions of the plasma. A typical magnetic safety factor profile from between sawteeth is shown as a function of the minor radius in figure 2(c) with the radial location of the rational surface for the first 10 $m = 1$ modes and all of the $m = 0$ modes indicated. The relatively large amplitude and global structure of the magnetic fluctuations suggests that many overlapping magnetic islands are present and the magnetic field will be largely stochastic, even away from the sawtooth crash. The rapid redistribution of current density that occurs at the sawtooth crash leads to a significant change in the magnetic equilibrium and large transient electric fields. To study fast ion dynamics in the presence of a broad-spectrum of tearing mode activity, the full orbit following random ion orbits (RIO) code has been developed. RIO,

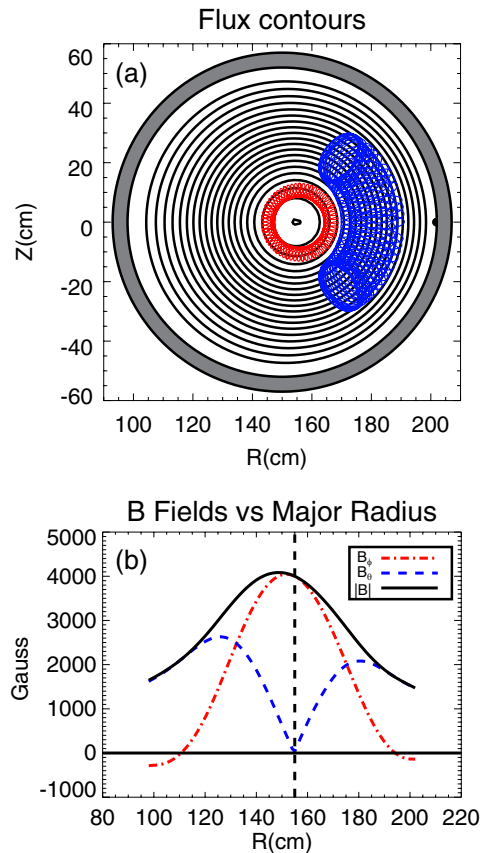


Figure 1. Panel (a) shows a set of typical flux surfaces for an RFP equilibrium in MST. The contours of constant flux are shown in black (note that they strongly resemble a set of shifted circles). Example poloidal projections of a passing (red) and a trapped (blue) 25 keV hydrogen ion trajectory are also shown. The conducting shell is indicated in grey and the half round outboard limiter is shown at the outboard mid-plane in black. Note that the last closed flux surface is not shown. Panel (b) shows the toroidal component (red dashed-dotted), poloidal component (blue dashed), and magnitude (black solid) of the equilibrium magnetic field as a function of major radius (with a vertical dashed black line marking the magnetic axis) from the MSTFit equilibrium reconstruction code.

which has been used in the past to inform fast ion studies on MST [13, 14], is now capable of taking the time evolving electric and magnetic fields for both the equilibrium and fluctuations as input. This allows for a detailed analysis of the impact of the sawtooth crash on the fast ion distribution. Furthermore, slowing down, pitch angle scattering and charge exchange effects are taken into account by tracing the charged particles through a parameterized background plasma. This can be done in either a cylindrical or a shifted circle toroidal geometry. By coupling RIO to the output of the 3D visco-resistive MHD code DEBS [15], which has now been run at experimentally relevant parameters [16], an assessment of the effects of the RFP sawtooth on the fast ion dynamics can be made. Note that while this work focuses on using RIO+DEBS to look at the RFP magnetic geometry, RIO can be used to look at any axisymmetric magnetic geometry where the magnetic equilibrium is well described by a set of nested circles. Furthermore, one could relatively easily couple the output of any MHD code to the input for RIO, DEBS is simply a code that is well suited for studying the RFP.

This work contains a detailed description of the RIO code as well as some initial results of particle tracing through a sawtooth event at MST parameters. Section 2 contains a general description of the code. Section 3 contains a description of the physics model used to compute the frictional drag, pitch angle scattering, and charge exchange effects on the test particles. Section 4 describes how the time evolving equilibrium and fluctuating fields are input into RIO and how this has been interfaced with the DEBS code. Finally, section 5 shows some initial results from particle tracing of neutral beam born ions in both a static background of broad-spectrum tearing modes and the time evolving magnetic and electric fields through a sawtooth event. In the latter case, significant particle energization, consistent with experimental measurements, is observed.

2. Description of numerics

RIO solves the Lorentz equation for charged particle motion in electromagnetic fields including collisional drag using the Hamiltonian formalism. We use Hamilton's equations, which in Cartesian coordinates are:

$$\begin{aligned} \frac{d\vec{p}}{dt} &= -\frac{\partial H}{\partial \vec{q}} - m_f v_d \frac{\partial H}{\partial \vec{p}}, \\ \frac{d\vec{q}}{dt} &= \frac{\partial H}{\partial \vec{p}}, \end{aligned} \quad (1)$$

where the Hamiltonian is $H = (\vec{p} - e_f \vec{A}/c)^2/(2m_f) + e_f \Phi$, m_f and e_f are the test particle mass and charge, v_d is the drag or slowing down rate due to collisions with the background plasma, \vec{q} is the generalized coordinate vector, \vec{p} is the generalized momentum vector, \vec{A} is the magnetic vector potential, and Φ is the electric potential. After performing a canonical transformation to generalized toroidal coordinates (and conjugate momenta), the equations are solved using a Runge–Kutta–Fehlberg scheme [17] in order to obtain the time evolution of the test particles position and velocity.

MST has a flux geometry that, due largely to the circular cross section of the close fitting conducting shell, is well approximated by a set of shifted circles. Furthermore, the RFP equilibrium is well modelled by a periodic cylinder with toroidal effects being less significant than a similarly sized tokamak. In fact, large scale MHD simulations of the RFP in a periodic cylinder geometry have been shown to reproduce many of the dynamics observed in the experiment [18]. Single fluid MHD simulations of MST at experimentally relevant parameters have shown quasi-periodic sawtooth activity and yield the time varying electric and magnetic fluctuation profiles. RIO is designed to take this cylindrical field and map it onto set of orthogonal generalized coordinates that are then cast as either a periodic cylinder or a shifted circle toroidal geometry. Cast in this way, one can easily switch the calculation of the particle trajectory from cylindrical to toroidal coordinates in order to gain a sense of the trapping effects. This also allows for realistic modelling of tangentially injected beam born fast ions in either geometry. Generally, neutral particles are injected in the toroidal geometry and their ionization location and pitch are calculated using a Monte-Carlo method. The particle trajectories can then be traced in

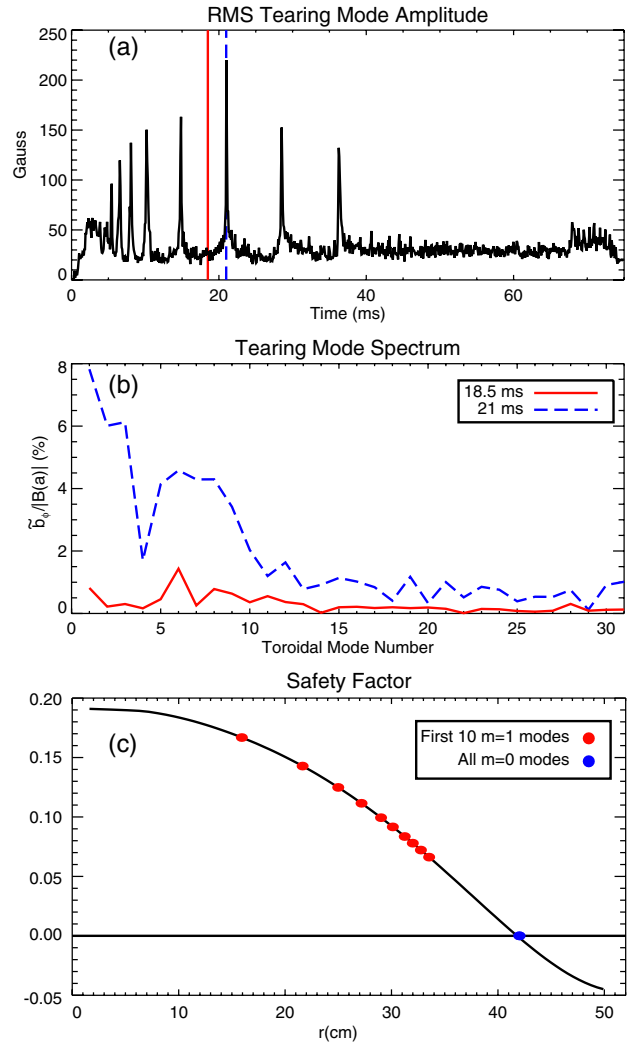


Figure 2. The top plot (a) show the time evolution of the RMS amplitude of the toroidal magnetic fluctuations (measured by a toroidal array of B-dot coils) over the course of a single MST discharge. Note the current flattop is ~ 20 – 40 ms. The middle plot (b) shows the fluctuation spectra at 18.5 ms (red solid) and during the sawtooth crash at 21 ms (blue dashed). The bottom plot (c) shows a typical magnetic safety factor profile with the radial position of the rational surfaces for the first 10 $m = 1$ and all the $m = 0$ modes indicated.

the toroidal geometry, or the ionization location and pitch can be mapped back to the cylindrical geometry. This mapping can be thought of as changing the tangential path of the injected neutral particles in the toroidal geometry to a curved path in the cylindrical geometry. In this way, a realistic fast ion deposition can be used in either geometry.

3. Description of particle interactions

The fast particles interact with the background plasma in many ways, several of which are accounted for in RIO. The first is simply collisional drag. The classical collisional drag rates are used to account for the drag on the test particles due to the background species [19]. We account for the Maxwellian averaged collisional drag from the background electron, bulk ion, and an arbitrary number of impurity ion species. Note that for the results show in section 5 we consider only the bulk ion

and electron collisions. The total drag, v_d , is simply the sum of the drag on the test particle due to each of the background species. For typical MST parameters the drag time for a 20 keV ion ($1/v_d$) is about 70 ms. The profiles for the neutral particles, electrons, and bulk and impurity ion temperature and density are generally approximated as radial profiles of the form $1 - (r/a)^\alpha$. The electron density is determined through quasi-neutrality. This allows for a self-consistent calculation of the slowing down due not only to the bulk ions and electrons, but an arbitrary number of impurity ion species as well. This is also how the ambipolar potential, which is part of the Φ term in the Hamiltonian, is specified.

Besides causing the drag that is taken in to account in the dynamic equations, the collisions generate pitch angle scattering that have to result in the following ensemble-average changes [19]:

$$\frac{d}{dt} \langle \delta V_{\parallel}^2 \rangle = \sum_{\xi=e,i,\dots} V_f^2 v_{\parallel}^{f|\xi}, \quad (2)$$

$$\frac{d}{dt} \langle \delta V_{\perp}^2 \rangle = \sum_{\xi=e,i,\dots} V_f^2 v_{\perp}^{f|\xi},$$

where V_f is the test particle velocity while v_{\parallel} and v_{\perp} are the total parallel and perpendicular scattering rates in velocity space. The total scattering rates are obtained by summing the standard scattering rates due to the test particle interaction with the various background species. Including the drag and pitch angle scattering in this way self-consistently generates the transition from slowing down to pitch angle scattering as the dominant effect on the test ions as they slow down below the critical energy. The scattering process as well as the charge exchange process are simulated using the Monte-Carlo approach. The latter allows for neutral beam injection from a synthetic neutral beam injector (NBI) with realistic divergence and injection angle characteristics, and for self-consistent calculation of the charge exchange loss.

4. Description of DEBS fields

RIO can take time varying electric and magnetic field information for both the equilibrium and fluctuations as input. Since the equations of motion are cast in terms of the potentials \vec{A} and Φ , it is actually these potentials that must be provided as input. We assume that the 3D fields can be written as follows (with only the vector potential shown here for brevity):

$$\vec{A} = \sum_{\alpha=1}^M \epsilon_{\alpha} \vec{A}_{\alpha}[r, t] e^{i(m_{\alpha}\theta + n_{\alpha}\phi)} + c.c. \quad (3)$$

with m_{α} and n_{α} as integer poloidal and toroidal mode number for each harmonic considered. When the magnetic (and electric) fields are supplied, as is the case when interfacing with the DEBS code, the potential fields are computed and the coefficients A_{α} (and similarly Φ_{α}) are chosen to provide the best approximation of the input data. The coefficients ϵ_{α} can be adjusted at run time and are used to provide agreement with experimental data for different experimental discharges of interest or to test the effect of raising and lowering specific mode amplitudes on confinement. It should

be noted that the inductive electric field is always computed self-consistently when the magnetic field is evolved in time, with any discrepancies between this and the supplied electric field accounted for in the Φ term in the Hamiltonian.

The input field can not possibly be given at every point of interest for the calculation of the particle trajectory, so the input field is preprocessed in order to generate a set of piecewise smooth functions of radius and time which are used to compute the field. These functions take one of three user selectable forms: a piecewise quadratic, a smoothed piecewise quadratic, and a piecewise gaussian fit. Because of the close fitting shell in MST, we also correct the fields to ensure that B_r goes to zero at the conducting wall and are represented in a form that identically satisfies $\vec{\nabla} \cdot \vec{B} = 0$. In the case of a resistive shell, known error fields, or some other non-ideal boundary condition, this feature can be turned off and the B_r will be set to the interpolated value of the provided B_r at the boundary. The approximate interpolation is done in both radius and time for each mode. This allows each mode to be independently scaled to measurements from MST or artificially changed to approximate scenarios that have not been simulated, such as pulsed parallel current drive (PPCD) and quasi-single helicity (QSH).

The ability to take a dynamically evolving field is critical for understanding the effects of sawteeth on the fast ion distribution. At the sawtooth crash, the magnetic fluctuations grow rapidly, redistributing current and rapidly altering the equilibrium magnetic field. The toroidal field on axis, for example, can change by 200 G in about 100 μ s. The changing magnetic field leads to a large transient inductive electric field in the core region of the plasma [7, 20]. Figure 3 show the simulated time evolution of the equilibrium magnetic and electric fields through a sawtooth crash from DEBS simulations run at parameters matching those of 400 kA standard discharges in MST. The fields change dramatically around the sawtooth crash. To get an accurate sense of the effect of this change on the fast ions, the full time evolving fields are required in the simulation. Furthermore, while it has been established that fast ions are well confined in standard RFP discharges, sufficiently high levels of fluctuations for a sufficient duration are expected to lead to fast ion loss. This code allows the amount and location of the fast ion loss to be determined self-consistently.

5. Results

The code has successfully modelled several interesting cases in MST, reproducing some of the observed behavior. In the first case we consider, five high pitch (small pitch angle) test ions are launched at 25 keV at various locations along the minor radius. The equilibrium and fluctuating magnetic field used in RIO is from a single time slice of a DEBS simulation. No electric field information was included (i.e. $\Phi = 0$). This allows a basic assessment of the effect of tearing modes on the fast ion confinement and we find that, despite relatively poor thermal ion confinement, fast ions are well confined in the core region of the plasma. In the second case (also without electric field information), we inject 10^4 neutral deuterium test particles over 1 ms (to simulate a beam blip from the 1 MW neutral beam injector) into a static background magnetic field with and

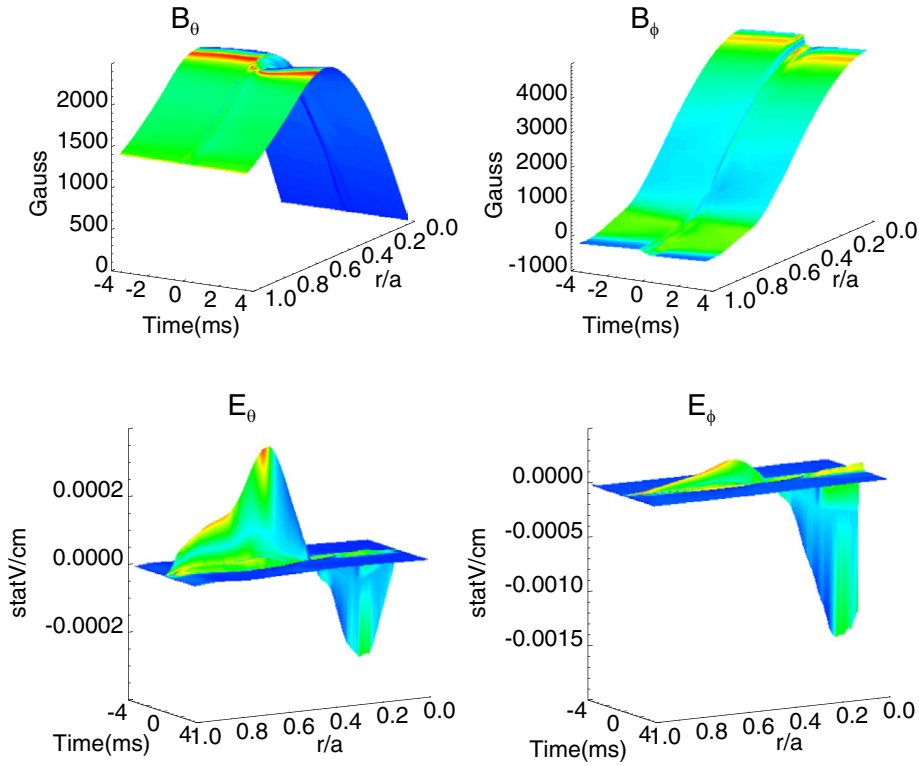


Figure 3. Magnetic and electric field profile evolution through a sawtooth crash (time = 0).

without fluctuations. The two sets of particles are traced for 10 ms from the end of the injection phase and then compared in order to assess the effect of broad-spectrum tearing modes on the fast ion distribution. In the third case, we inject 10^4 neutral deuterium particles from the synthetic NBI into the full time evolving magnetic and electric field taken from the simulations in order to assess the impact of the RFP sawtooth event on the fast ion distribution. For the cases with 10^4 particles, the runs take 2 to 5 days on 200 Intel Xenon cores in a mixed cluster of 16 X5570 at 2.93 GHz, 10 X5550 at 2.67 GHz, and 24 L5520 at 2.26 GHz (all quad cores). It should be noted that in all cases the fast ions are treated as test particles. This assumption is made for two reasons. First, we have observed no indication of fast particle driven instabilities or any other significant reaction of the background plasma for short beam pulses (under 3 ms). Second, we currently have no way to couple information from the fast ion distribution back into the DEBS code. It should also be noted that the number of modes used in the full orbit calculation is reduced from the hundreds of modes in the DEBS simulation to the 64 largest modes. These are primarily the low n , $m = 0, 1$, and 2 modes. This is done for computational expedience and is not a fundamental limitation of the code.

5.1. Fast ion confinement in a stochastic magnetic field

Tangentially injected fast ions have been observed to be well confined in MST despite a strongly stochastic magnetic field [13, 21, 22]. This has been understood to be largely due to drift orbit averaging, which gives the fast ion guiding centres their own effective safety factor ($q_{\text{fi}} = rV_{\phi}/RV_{\theta} = f_{\phi}/f_{\theta}$ where f_{ϕ} and f_{θ} are the toroidal and poloidal transit frequencies) that is substantially shifted from the magnetic safety factor

($q_m = rB_{\phi}/RB_{\theta}$). The effective safety factor profile for the fast ions will have its own analogous resonant locations and island widths at rational values of q_{fi} [13, 14, 23]. The linear approximation for q_{fi} , as shown in [14], is:

$$q_{\text{fi}} \approx q_m + \frac{S_{\parallel} V}{B_{\theta}^2 \Omega} \frac{2(1 - \mu\Omega) B_{\theta}^2 - r\mu\Omega'}{2R\sqrt{1 - \mu\Omega}} \quad (4)$$

where $S_{\parallel} = \frac{\vec{V} \cdot \vec{B}}{|\vec{V} \cdot \vec{B}|}$ is the sign of V , $\Omega = \frac{eB}{mc}$ is the gyro-frequency, $\mu = \frac{E_{\perp}}{E_0\Omega} = \frac{V_{\perp}^2}{V^2\Omega}$ is the ratio of the perpendicular energy to the total energy divided by the gyro-frequency, and the primes are radial derivatives. Note that equation (4) is only valid for moderate to high pitch ions. As the pitch approaches zero, the poloidal transit frequency becomes poorly defined and the analogy to the magnetic field behavior breaks down. For co-injected fast ions in MST, the effect of the drift orbit averaging is to raise q_{fi} above q_m . A typical q_m profile from a DEBS simulation of MST is shown in black in figure 4 with the magnetic island widths for the $m = 1$, $n = 5-31$ modes shown centred around their resonance radius (i.e. where $\vec{k} \cdot \vec{B} = 0$). Given MST's q profile, the drift orbit effects move the resonant locations for the modes radially outward and away from the peak in the magnetic perturbation amplitude. These two factors tend to make the islands in the fast ion trajectories smaller than the corresponding magnetic island for a given mode, helping to limit stochastic fast ion orbits to the outer part of the plasma. Assuming the fast ion profile is strongly core peaked, this effect explains the relatively long fast ion confinement times observed in MST. The q_{fi} profile is shown in red in figure 4 with the approximate $m = 1$, $n = 5-16$ island widths plotted as well. This q_{fi} profile is for a pitch of 1 (co-current) fast ion. As the pitch is increased, the difference between q_m and q_{fi} increases,

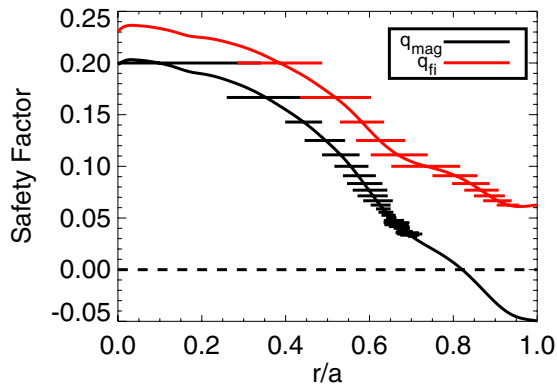


Figure 4. Magnetic safety factor (black) and effective safety factor of the fast ion guiding centre for a pitch = 1 (co-current), 25 keV hydrogen ion (red). The approximate island widths for the $m = 1$ modes are also shown.

with the largest increase being in the core region. This suggests that core localized ions of any positive pitch will be relatively unaffected by the magnetic perturbations resonant in the core region of MST unless the mode amplitudes get very large. By launching particles at different radial locations and plotting the guiding centre location of each point as it crosses the $Z = 0$ plane, as in figure 5, we can easily see the effect of these islands on the fast ion trajectories. The particles launched in the core (orange and yellow) clearly have well confined orbits with the guiding centres being largely unaffected by the remnant $m = 1$, $n = 5$ magnetic island. The particles launched at larger radius (purple and green) have their own $n=5$ resonance despite the highly stochastic magnetic field in this region. Moving still further out in radius (red), the fast ion trajectories eventually become stochastic and the ions sample a significant fraction of the minor radius until they are eventually lost.

5.2. Effect of broad-spectrum tearing modes on beam injected ions in a toroidal geometry

Since the RIO code is capable of modelling charge exchange processes given the experiment-like temperature and density profiles, the beam can be simply modelled as a distribution of neutral particles launched towards the plasma at a given energy. This is important as it assesses the fraction of the actual beam injected particles that go into well confined orbits (as opposed to stochastic orbits that will be rapidly lost). The geometry and divergence of the NBI on MST is used and the fast ion deposition is computed. These simulations have been performed using deuterium ions injected into a background plasma with static electron, deuterium ion, and deuterium neutral temperatures and densities, all of which match 400 kA standard plasmas in MST. The resulting beam deposition is roughly consistent with TRANSP/NUBEAM predictions, but has the advantage that it correctly models the beam deposition near the $q = 0$ surface. Here we have modelled a 1 ms 50 A 25 keV beam blip with 10^4 test particles. These particles are injected into a static magnetic field taken from the DEBS simulation 3 ms before a sawtooth crash (similar to the time slice indicated in figure 2 by the solid red line). No electric field was applied in this case. Figure 6(a) shows the initial deposition of the test particles in a toroidal cross section while figure 6(b) shows the pitch distribution of the initial deposition. The sign of

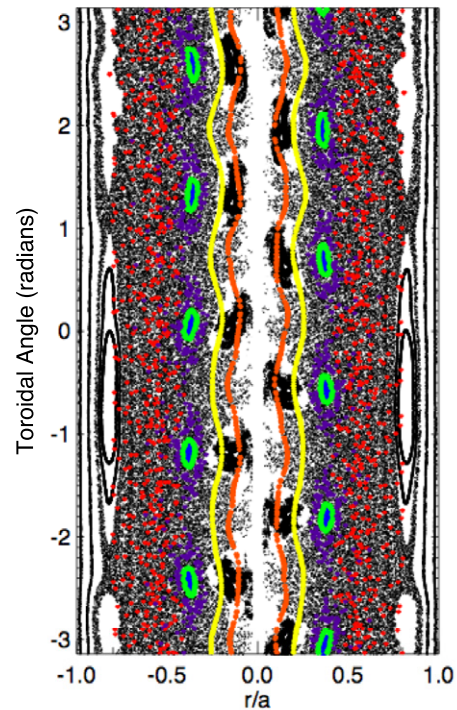


Figure 5. Toroidal puncture plot of the magnetic field (black) and five separate 25 keV hydrogen fast ion trajectories launched at various radii (coloured). The core-most ions (orange and yellow) are clearly well confined while those launched in the mid radius (red) are stochastic.

the pitch is such that particles propagating in the co-current direction have positive pitch and counter propagating particles have negative pitch. Note that there are a significant number of low pitch (large pitch angle) ions deposited near the $q = 0$ surface. Many of these are lost promptly, but some are confined throughout the simulation.

The effect of the spectrum of tearing modes on the fast ion distribution is subtle. Figure 7(a) shows the fast ion density profile 10 ms after injection for a case without tearing modes (black solid) and a case with the 64 highest amplitude magnetic fluctuations (red dashed) while figure 7(b) shows the relative change in density between the two cases. As expected, the core fast ion density is nearly identical with and without magnetic modes. However, at mid-radius the fast ion density is reduced by approximately a factor of two due to enhanced losses from the stochastic trajectories that the particles begin to experience in this region [24]. In other words, once the particles begin to interact with the modes, they traverse more of the minor radius of the plasma. When the perturbations to the ion orbit from one mode overlap with the neighboring perturbation, the radial extent of the orbit is further enhanced until the particle orbit makes it all the way to the edge of the device and the particle is lost. While the non-trivial enhancement to the fast particle loss in the mid-radius is expected given the single particle trajectories shown in the previous example, it is encouraging that this loss is small in terms of absolute density. This result suggests that the number of beam ions that are quickly lost due to tearing mode activity is relatively small and that most of the injected fast ions make it into well confined orbits. It is also worth noting that both of the curves shown in figure 7(a) are

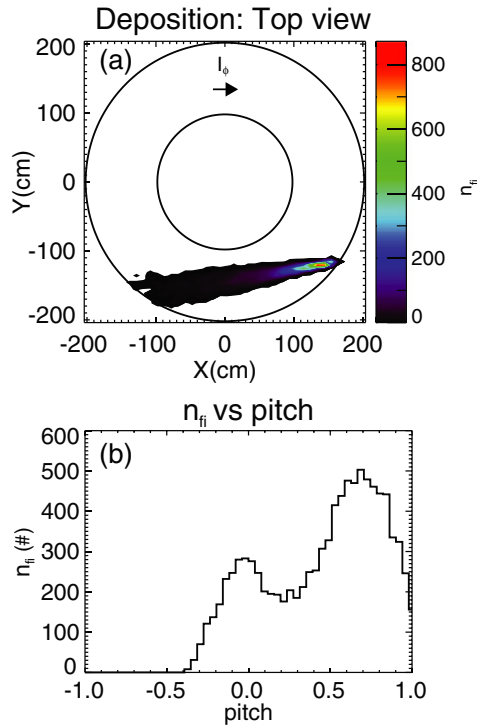


Figure 6. Initial deposition of beam injected fast ions in (a) space and (b) pitch (positive is co-current, negative is counter current). The initial pitch deposition peaks at ~ 0.68 . Later in time the pitch is much more strongly peaked at ~ 0.8 .

made up all most entirely of passing particles with the relative number of trapped particles being about 5% in both cases. This is likely simply do to the injection geometry leading to preferential ion deposition into passing orbits. A separate study of the effects of tearing modes on radially injected ions is needed in order to ascertain the effect of tearing modes on a large population of trapped ions, but this is left for future work as MST does not currently have any plans for high power radial neutral beam injection.

5.3. Effect of the sawtooth crash on the fast ion distribution

Finally, RIO is also capable of taking the full time evolving electric and magnetic field from DEBS as input. In the experiment, we often see evidence of significant acceleration of beam injected ions (about 5 keV for 20 keV fast ions, or $\sim 25\%$) on a tangentially viewing neutral particle analyser (called the Advanced Neutral Particle Analyser, or ANPA) [25, 26]. By evolving both the magnetic and electric fields in time we are able to track test particles throughout the sawtooth event to gain detailed information on how the fast ion population is modified by these strong MHD events.

The setup for this simulation is the same 400 kA background plasma and 1 ms deuterium beam blip as the last example, but now the fields are evolved in time as the injected ions circulate. It should be noted that while the effect of impurity ion species on the test particles can be modelled, none were used for this case. It should also be noted that fast ions in high concentration can excite magnetic instabilities that are resonant with the ion motion and cause rapid fast ion transport [27, 28]. These effects have been ignored here because we are modelling a short blip of NBI and have not observed any

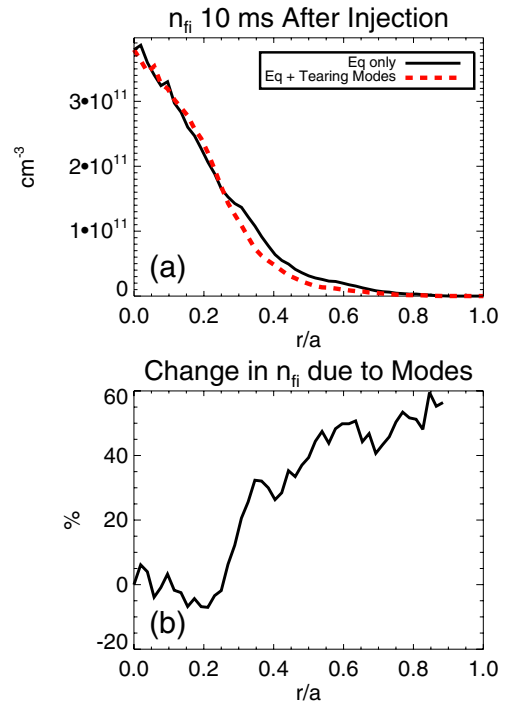


Figure 7. Fast ion density with and without tearing modes (a) and relative difference between the two profiles (b). Note that there were no test particles outside $r/a \approx 0.9$ in the simulation.

evidence of fast particle driven instabilities in similar beam blip experiments performed on MST. The resulting fast ion density and β profiles have relatively steep gradients, possibly approaching marginal stability, but here we are just considering the effects of tearing modes and the mean field evolution on the fast ions. Figure 8 shows the fast ion density from 200 μ s before the sawtooth crash in black and 200 μ s after the sawtooth crash in red dashed. While the maximum relative change in the fast ion density occurs in the mid radius, which is expected as this is where a largest number of tearing modes are resonant, the most striking feature of figure 8 is the $\sim 40\%$ reduction in the fast ion density in the core region. The sawtooth crash causes direct loss of many of the particles that were confined in the mid radius region and radial transport of many of the fast particles that were confined in the core region. In absolute terms, the net result is a somewhat small change in the absolute density in the mid-radius while the core fast ion density is substantially reduced. The physical mechanism that causes this behavior is, again, simply resonant interaction of the particles drift orbit with the MHD modes leading to an enhanced radial extent to the particle orbit. Recall that at the sawtooth crash the magnetic modes become very large all across the plasma. In the mid-radius, the drift orbit sees overlapping islands and it's trajectory becomes chaotic. This orbit eventually intersects with the wall and the particle is lost. The ions that are initially core localized see a single large island that spreads them out radially. As the fluctuations grow, the edges of this island can start to overlap with the next neighboring island. In this way, many of the core particles can eventually make it into the stochastic region. As the fluctuation amplitudes decrease after the sawtooth crash, the particles that have not yet been lost from the mid radius region will be confined there.

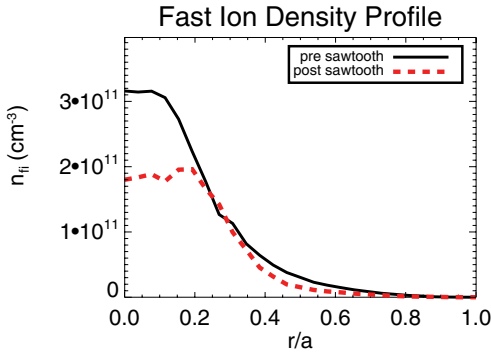


Figure 8. Fast ion density profile before (black solid) and after (red dashed) the sawtooth crash.

Finally, it should also be noted that nearly all of the beam injected particles are passing particles with trapped particles representing less than 5% of the total number of test particles. The fraction of trapped particles decreases at the sawtooth crash, dropping to about 2% after the crash. The trapped particles tend to reside in the mid radius of the plasma where most significant losses are and therefore, unsurprisingly, most of the trapped particles ($\sim 75\%$) are lost at the sawtooth crash. Most of the remaining fast ions are de-trapped by the large parallel electric fields seen at the sawtooth crash. Only $\sim 5\%$ of the particles that were trapped before the crash are still trapped after the crash. The majority of the particles found in trapped orbits after the sawtooth crash were passing particles that, through a combination of radial transport and slowing down, become trapped. That said, most of the particles transported out to the mid radius remain in passing orbits.

Interestingly, despite the significant drop in fast ion density in the core, the energization of the fast ions that remain in the core region leads to a relatively small change in the core averaged fast ion β . The local fast ion β is defined as $\beta(r) = \sum_{i=0}^n \frac{m_i V_i^2 / 2}{B_i^2 / 8\pi} \frac{1}{4\pi^2 R r dr}$ where the sum is over the number of fast ions at each radial position. Figure 9 shows the fast ion β profile as a function of minor radius from before and after the sawtooth crash. The average β inside $r/a = 0.2$ is relatively constant (only dropping about 12%) while the mid radius shows a significant drop (over 50%). Part of the change in the β_{fi} profile is due to a few percent change in the toroidal magnetic field profile, which decreases on axis and increases in the mid radius at the sawtooth crash. However, the majority of the change is from ion acceleration due to a parallel electric field. The E_{\parallel} profile generated at the sawtooth crash crosses through zero in the mid radius causing acceleration in the core and deceleration in the mid radius and edge [29]. Surprisingly, this simulation suggests that the sawtooth can actually briefly enhance the β_{fi} gradient in the transition region around $r/a \approx 0.3$ rather than flattening it. On average, the fast ions that remain in the core region of the plasma gain parallel energy leading to an increase in both the average energy and average pitch. Figure 10 shows the fast ion pitch and energy distribution for the particles inside $r/a = 0.2$ from before and after the sawtooth crash. The preferential acceleration in the parallel direction shifts the average pitch from ~ 0.8 to ~ 0.9 . The average energy increase in these core localized fast ions is about 4 keV, or $\sim 22\%$, which is roughly consistent

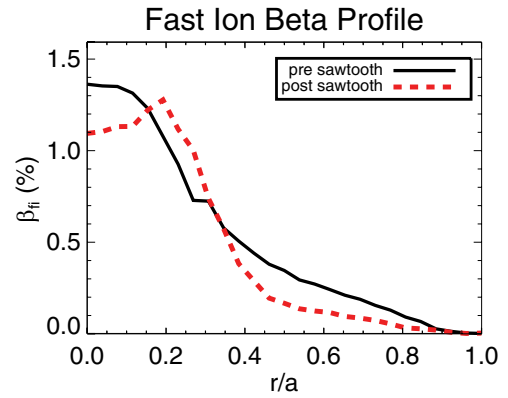


Figure 9. Fast ion β profiles from before (black solid) and after (red dashed) the sawtooth crash.

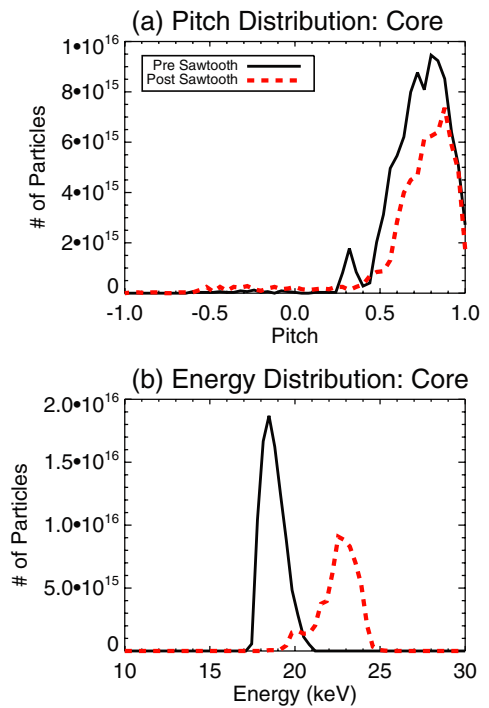


Figure 10. Core fast ion (a) pitch and (b) energy before (black solid) and after (red dashed) the sawtooth crash. The pitch increases due to acceleration from the mean E_{\parallel} and average energy increases by about 5 keV.

with the ANPA measurements of beam injected ions on MST (see, for example, figure 6 in [25]). While this is consistent with experimental measurement, we have not yet attempted to make a synthetic NPA to directly compare the simulation to the measurement, though we hope to do so in the near future. The enhancement in the pitch is also seen in the particles resonant in the mid radius, which again is consistent with the smaller than expected number of trapped particles seen in the mid radius after the sawtooth crash.

While the agreement in the fast ion energization is encouraging and the observed fast ion dynamics are interesting, it is important to stress that these results are not a prediction of the fast ion density, β , or energy expected in the experiment, but rather an exercise exploring the possible effects of large variations in the fields on a distribution of fast ions. There

are no error bars on any of the results presented because the primary uncertainty is likely due to uncertainty in the input values. The sensitivity of these results to the various input profiles is currently unknown. Sensitivity studies and a detailed comparison to observable quantities such as the neutron flux and neutral particle analyser measurements be the subject of future work.

6. Conclusions

We have developed a full orbit particle tracing code that is capable of taking the full magnetic and electric field information from MHD simulations as input. This allows for a detailed study of the effect of tearing modes and magnetic stochasticity on fast ion confinement. Furthermore, the ability to evolve the magnetic and electric fields in time allows the detailed study of transient events on the fast ion distribution. Initial results show that core localized fast ions are well confined, which is due to drift orbit averaging over the stochastic magnetic field in these RFP plasmas. The broad-spectrum tearing mode activity in MST, while likely substantially reducing the neutral beam injected fast ion density in the mid-radius, has little effect on the total fast particle density for the co-injected neutral beam due to the strongly core peaked fast ion density profile. During a sawtooth event, the large magnetic perturbations cause substantial fast ion transport with the core localized ions moving out in radius and the mid-radius ions being lost. However, despite a substantial reduction in the core fast ion density, the fast ion β is largely maintained due to parallel acceleration of the confined ions. This acceleration leads to a roughly 20% increase in average energy, which is consistent with experimental results from MST.

Acknowledgments

The authors would like to thank Mark Nornberg and Gennady Fiksel for many helpful suggestions regarding this work. This work is supported by the United States Department of Energy under grant number DE-FCO2-05ER54814 and the Russian Federal Ministry of Science and Education.

References

- [1] White R.B. and Chance M.S. 1984 Hamiltonian guiding center drift orbit calculation for plasmas of arbitrary cross section *Phys. Fluids* **27** 2455
- [2] Egedal J. 2000 Drift orbit topology of fast ions in tokamaks *Nucl. Fusion* **40** 1597–610
- [3] Clark J.L., Capecchi W., Egedal J. and Anderson J.K. 2013 Fast ion orbit topology in the reversed-field pinch *55th Annual Meeting of the APS Division of Plasma Physics (Denver, CO)* vol 58 CP8.00073
- [4] Kramer G.J., Budny R.V., Bortolon A., Fredrickson E.D., Fu G.Y., Heidbrink W.W., Nazikian R., Valeo E. and Van Zeeland M.A. 2013 A description of the full-particle-orbit-following SPIRAL code for simulating fast-ion experiments in tokamaks *Plasma Phys. Control. Fusion* **55** 025013
- [5] Dexter R.N., Kerst D.W., Lovell T.W., Prager S.C. and Sprott J.C. 1991 The Madison Symmetric Torus *Fusion Technol.* **19** 131–9
- [6] Prager S.C. *et al* 1990 First results from the Madison Symmetric Torus reversed field pinch *Phys. Fluids B: Plasma Phys.* **2** 1367
- [7] Ding W., Brower D., Craig D., Deng B., Fiksel G., Mirmov V., Prager S., Sarff J. and Svidzinski V. 2004 Measurement of the Hall dynamo effect during magnetic reconnection in a high-temperature plasma *Phys. Rev. Lett.* **93** 4–7
- [8] Fitzpatrick R., Guo S.C., Den Hartog D.J. and Hegna C.C. 1999 Effect of a resistive vacuum vessel on dynamo mode rotation in reversed field pinches *Phys. Plasmas* **6** 3878
- [9] Anderson J.K., Forest C.B., Biewer T.M., Sarff J.S. and Wright J.C. 2004 Equilibrium reconstruction in the Madison Symmetric Torus reversed field pinch *Nucl. Fusion* **44** 162–71
- [10] Ho Y.L. and Craddock G.G. 1991 Nonlinear dynamics of field maintenance and quasiperiodic relaxation in reversed-field pinches *Phys. Fluids B: Plasma Phys.* **3** 721
- [11] Hokin S. *et al* 1991 Global confinement and discrete dynamo activity in the MST reversed-field pinch *Phys. Fluids B: Plasma Phys.* **3** 2241
- [12] Taylor J.B. 1986 Relaxation and magnetic reconnection in plasmas *Rev. Mod. Phys.* **58** 741
- [13] Fiksel G., Hudson B., Den Hartog D., Magee R., O’Connell R., Prager S., Beklemishev A., Davydenko V., Ivanov A. and Tsidulko Yu. 2005 Observation of weak impact of a stochastic magnetic field on fast-ion confinement *Phys. Rev. Lett.* **95** 125001
- [14] Hudson B. F. II 2006 Fast ion confinement in the reversed-field pinch *PhD Thesis* University of Wisconsin, Madison
- [15] Schnack D.D., Barnes D.C., Mikic Z., Harned D.S. and Caramana E.J. 1987 Semi-implicit magnetohydrodynamic calculations *J. Comput. Phys.* **70** 330–54
- [16] Reusch J., Anderson J., Den Hartog D., Ebrahimi F., Schnack D., Stephens H. and Forest C. 2011 Experimental evidence for a reduction in electron thermal diffusion due to trapped particles *Phys. Rev. Lett.* **107** 1–5
- [17] Forsythe G.E., Malcolm M.A. and Moler C.B. 1977 *Computer Methods for Mathematical Computations* (Englewood Cliffs, NJ: Prentice-Hall)
- [18] Ortolani S. and Schnack D.D. 1993 *Magnetohydrodynamics of Plasma Relaxation* (Singapore: World Scientific)
- [19] Trubnikov B.A. 1965 Particle interactions in a fully ionized plasma *Rev. Plasma Phys.* **1** 105
- [20] Deng B.H., Ding W.X., Brower D.L., Almagri A.F., McCollam K.J., Ren Y., Prager S.C., Sarff J.S., Reusch J.A. and Anderson J.K. 2008 Internal magnetic field structure and parallel electric field profile evolution during the sawtooth cycle in MST *Plasma Phys. Control. Fusion* **50** 115013
- [21] Liu D. *et al* 2011 Neutral beam injection experiments in the MST reversed field pinch *12th IAEA Technical Meeting on Energetic Particles in Magnetic Confinement Systems (Austin, TX, 2011)* pp 1–8
- [22] Anderson J.K. *et al* 2013 Fast ion confinement and stability in a neutral beam injected reversed field pinch *Phys. Plasmas* **20** 056102
- [23] Gobbin M., White R.B., Marrelli L. and Martin P. 2008 Resonance between passing fast ions and MHD instabilities both in the tokamak and the RFP configurations *Nucl. Fusion* **48** 075002
- [24] Berk H.L., Breizman B.N., Fitzpatrick J., Pekker M.S., Wong H.V. and Wong K.L. 1996 Nonlinear response of driven systems in weak turbulence theory *Phys. Plasmas* **3** 1827
- [25] Eilerman S., Anderson J.K., Reusch J.A., Liu D., Fiksel G., Polosatkin S. and Belykh V. 2012 Time-resolved ion energy distribution measurements using an advanced neutral particle analyzer on the MST reversed-field pinch *Rev. Sci. Instrum.* **83** 10D302
- [26] Eilerman S. *et al* 2014 Ion runaway in the reversed-field pinch *Phys. Rev. Lett.* in preparation

- [27] Koller J. *et al* 2012 Fast-particle-driven Alfvénic modes in a reversed field pinch *Phys. Rev. Lett.* **109** 1–5
- [28] Lin L. *et al* 2013 Measurement of energetic-particle-driven core magnetic fluctuations and induced fast-ion transport *Phys. Plasmas* **20** 030701
- [29] Ennis D.A., Craig D., Gangadhara S., Anderson J.K., Den Hartog D.J., Ebrahimi F., Fiksel G. and Prager S.C. 2010 Local measurements of tearing mode flows and the magnetohydrodynamic dynamo in the Madison Symmetric Torus reversed-field pinch *Phys. Plasmas* **17** 082102